Quantitative Defect Reconstruction in Active Thermography for Fiber-Reinforced Composites

Sebastian GÖTSCHEL [1], Christiane MAIERHOFER [2], Jan P. MÜLLER [2], Nick ROTHBART [2], Martin WEISER [1]
[1] Konrad-Zuse-Zentrum für Informationstechnik Berlin (ZIB), Berlin, Germany
[2] BAM Bundesanstalt für Materialforschung und -prüfung, Berlin, Germany

Contact e-mail: goetschel@zib.de

Abstract. Carbon-fiber reinforced composites are becoming more and more important in the production of light-weight structures, e.g., in the automotive and aerospace industry. Thermography is often used for non-destructive testing of these products, especially to detect delaminations between different layers of the composite.

In this presentation, we aim at methods for defect reconstruction from thermographic measurements of such carbon-fiber reinforced composites. The reconstruction results shall not only allow to locate defects, but also give a quantitative characterization of the defect properties. We discuss the simulation of the measurement process using finite element methods, as well as the experimental validation on flat bottom holes.

Especially in pulse thermography, thin boundary layers with steep temperature gradients occurring at the heated surface need to be resolved. Here we use the combination of a 1D analytical solution combined with numerical solution of the remaining defect equation. We use the simulations to identify material parameters from the measurements.

Finally, fast heuristics for reconstructing defect geometries are applied to the acquired data, and compared for their accuracy and utility in detecting different defects like back surface defects or delaminations.

Introduction

Active thermography is a fast and contactless method for nondestructive testing of a wide range of structures. It is based on the generation of a non-stationary heat flux inside the object under investigation, and time-resolved measurements of its surface temperature by an infrared camera. Defects and inhomogeneity in the material with thermal properties differing from the surrounding material can be detected from spatial temperature differences within a particular time range. Often, quantitative information about such defects, like depth, residual wall thickness or lateral extent need to be extracted from the measurements. Models like PPT (pulse phase thermography) [1] and TSR (thermographic signal reconstruction) [2], considering solely the heat flow normal to the surface of the specimen, deliver a fast way to assess the size and to a certain extent the depth of the defect within the sample. Since they are based on analytical solutions of simplified models, they are well suited for practical applications.

For a more detailed inspection in order to obtain quantitative results, is strongly desirable to take lateral heat flows into account. A viable path to reconstruct the sub-surface defects of the specimen is to numerically solve the underlying PDE and optimize the geometric data and the thermal material parameters iteratively. This way to solve the inverse problem is computationally expensive, but paves the road to extract much more detailed information from the measurements, compared to the analytical reconstruction methods. In this contribution, we describe experiments, simulation and reconstruction methods for carbon-fiber reinforced composites.

1. Experiments

Two samples (produced by ZfL Haldensleben) have been investigated by flash thermography [3]. One sample consists of pure epoxy resin (the almost isotropic matrix material of CFRP), the other one of unidirectional CFRP. A photo of each specimen is shown in Fig 1. a) and b). The second specimen was produced using the RTM-light process. 34 layers of woven carbon filaments, having a weight of 140 g/m^2 were aggregated with their fibers in parallel (fiber orientation is in vertical direction in Figure 1 b). The layers are plain warp reinforced. At the surface two layers turned by 90° with respect to the rest of the layers are added. Finally, epoxy resin has been added under vacuum conditions inside a form. The sample has been stored for 24 h at a temperature of 50-60 °C. The layer structure can be clearly seen in Fig. 1 c). Both specimens have defined flat bottom holes of distinct diameter and depth machined on the sample – in a similar pattern. The holes serve as defined defects on the back side of the investigated flat surface and enable to assess the reconstruction process. The sample made of pure epoxy resin has an average thickness of 5.5 mm, the CFRP sample of 5.8 mm. Both samples have a dimension of 200 x 200 mm^2. The residual wall thickness of the holes, having diameters between 4 and 24 mm, amounts from 0.5 mm up to 4.2 mm. The surface of the sample made of epoxy resin was blackened using two layers of paint (Tetenal camera paint).

Time-resolved thermography has been carried out using flash excitation of the front surface to obtain information on the back side of the specimen. This represents a model case for non-destructive testing of materials. Four flash lamps (Hensel Studio Technik, EH PRO 6000), having 6 kJ energy each, are heating the plane surface. The flash lamps have a maximum radiation temperature of 5000 K, the main infrared (IR) part of the spectrum is mitigated by two PMMA-plates having a thickness of 8 mm. Thus the specimen is heated mainly by visible light within a short time. The light intensity of the flash lamps can be described with respect to time by an exponential decay function, the half time amounts to 2.0 ms. The flash duration has been measured using a photodiode (Thorlabs, PDA36A-EC) with metallic neutral density filters mounted on its front. The flash lamps are aligned for a homogeneous illumination of the sample surface. The main axis of the lamps is aligned in an angle of 15° relative to the normal to the front of the specimen, at a distance of 45 cm typically. The IR camera is positioned behind the gap between the flash lamps. The epoxy resin as well as the CFRP sample is supported by a frame made of corrugated board, which shields the IR camera from the flash light as well as thermally insolates the sample.

The IR camera (Infratec, ImageIR 9830), equipped with a 50 mm lens, records the temperature using a fast InSb-focal plane array in the spectral wavelength range of 3 - 5 µm. It has a maximal resolution of 1280 x 1024 pixels and the transient temperature of the specimen has been imaged at a frame rate of 10 Hz (full frame) and 180 Hz (half frame). For synchronization of the flash lamps with the camera a custom made active box (Infratec) is used. Calibration ranges for the temperatures from 0 - 60 °C (integration time of the sensor 640 µs) and 20 - 100 °C (integration time 260 µs) are used.

In addition to the epoxy resin or CFRP plates a blackened piece of silver mounted next to the sample is utilized to estimate the irradiation [4]. The energy density deposited on the surface amounts to $(0.27 \pm 0.01)\ J / cm^2$.

The specimens have been investigated using two configurations: the IR camera viewing the illuminated front surface of the sample (reflection configuration) for creating the experimental data to reconstruct the defects, as well as the IR camera viewing the back surface (transmission configuration). The latter set-up enables to measure the in-depth thermal diffusivity of the materials using the method of Parker et al. [3].

The images of the camera are saved in a binary file format of the Irbis3 software (Infratec). The transient signal, consisting of 2000 frames typically, is loaded into the programming language Matlab, in order to prepare the data for the numeric reconstruction method. A background image, taken before the flash heated the sample, is subtracted from the transient temperature signal. Only the frames recorded after the flash are used for the comparison to the simulation.

To determine the thermal lateral diffusivity on the surface of the epoxy resin and CFRP a distinct method is used. A laser (laserline LDM 500-20) is coupled into an optics generating a line focus. The beam waist has a Gaussian profile in x-direction (FWHM of 1 mm) and a homogeneous intensity distribution in y-direction (spreading over 36 mm). The optical axis of the caustics is aligned in an angle of 30° with respect to the surface normal of the specimen. The laser runs at a wavelength of 935 nm and illuminates the sample for 100 ms with a power of about 15 W. Due to the absorption of the IR laser light the sample is heated to temperatures up to 90 °C. A fast IR camera (Infratec, ImageIR 8300) measures the thermal signal in the MWIR range from 2-5 µm with a framerate of 180 Hz. A cooled InSb focal plane array, having 640 x 512 pixels in combination with a lens ($f / 2.0$, resolution $0.18\ mm / pixel$) is used to record the temporal evolution of the surface temperature, a calibration of 10-100 °C (485 µs integration time) is used. The protraction of the width of the hot area is utilized to obtain the in-plane diffusivity perpendicular to the laser line. The evaluation of the transient images is similar to the procedure developed by Bison et al. [5]. The thermal diffusivities measured are used as a parameter fed into the numerical reconstruction procedure. The results of the diffusivity measurements are shown in Table 2.

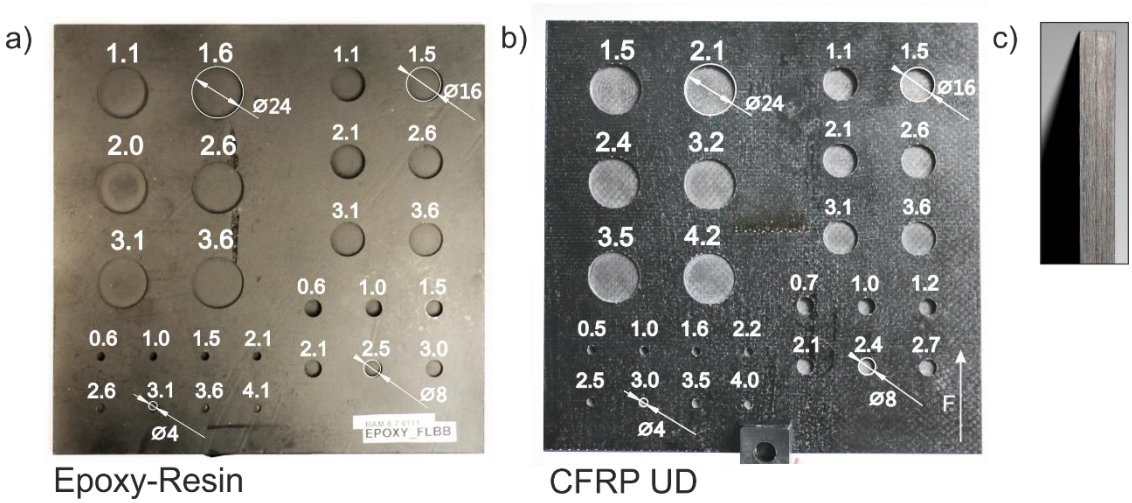

Fig. 1. Pictures of the specimen having flat bottom holes drilled into. The hole diameters are the same for a group of 6-8 holes and are marked in the picture (diameter given in mm). The residual wall thicknesses are shown with a number above the hole in mm. b) Epoxy-resin specimen b) CFRP sample, unidirectional layers holes drilled into the sample. c) A view from the side. The distinct layers of the CFRP material are clearly visible. The main direction of the fibers (except for the two surface layers) is marked with a white arrow designated with "F".

2. Simulation

2.1 Numerical solution

For PDE-based reconstruction methods, an accurate solution of the forward problem needs to be obtained in order to minimize the difference between measurements and simulation results. Here, the forward problem is given by the heat equation

$$\begin{aligned} \rho c \theta_t &= \operatorname{div}(\lambda \nabla \theta) \text{ in } \Omega \times (0,T) \\ \lambda \partial_n \theta &= Q + g(\theta) \text{ on } \partial\Omega \times (0,T) \\ \theta(0) &= \theta_0 \qquad \text{in } \Omega, \end{aligned}$$

where for CFRP UD the heat conductivity λ is anisotropic, i.e. higher in fiber direction along the y-axis than orthogonal to it. Heating by the flash lamps is included in the boundary condition via the heat flux Q. Additionally, $g(\theta)$ is a combination of convective and radiative heat transfer. As thermal diffusivity and heating time are very small compared to the surface area, the temperature exhibits a very thin boundary layer, which has to be represented accurately in the numerical solution by finite element methods. We use the hybrid analytic-numerical method developed in [6] to obtain accurate solutions in reasonable computing times. The implementation is done using the C++ finite element toolbox Kaskade7 [7].

2.2 Results

Exemplarily, Figure 2 shows a comparison of measurement and simulation showing of the spatial temperature distribution of the CFRP UD specimen. For the heat conductivity, we use averaged values computed according to [8], derived from the conductivity of fiber (9.4 W/(m K)) and matrix (0.2 W/(m K)), as well as the fiber volume fraction (52.6%), (see also Table 2). A calculation having high resolution considering single fibers is computationally far too expensive. As the layers are unidirectional (except for the top and bottom layer), we did not resolve individual layers. Around 142,000 tetrahedral elements with quadratic ansatz functions were used.

The colder rectangular area on the lower right corner in the measurements is due to a label with different thermal properties than the specimen itself, which is not included into the simulation. Also, in the beginning, influence of non-homogeneous heating is visible in the measurements. As its influence on the temperature evolution is rather small, this is neglected in the simulation. Overall, the simulation results show reasonably good agreement with the measurements. E.g., both data sets show the elliptic shapes of the thermal signature of the holes due to the anisotropic thermal diffusivity, which is higher in fiber direction of the unidirectional CFRP.

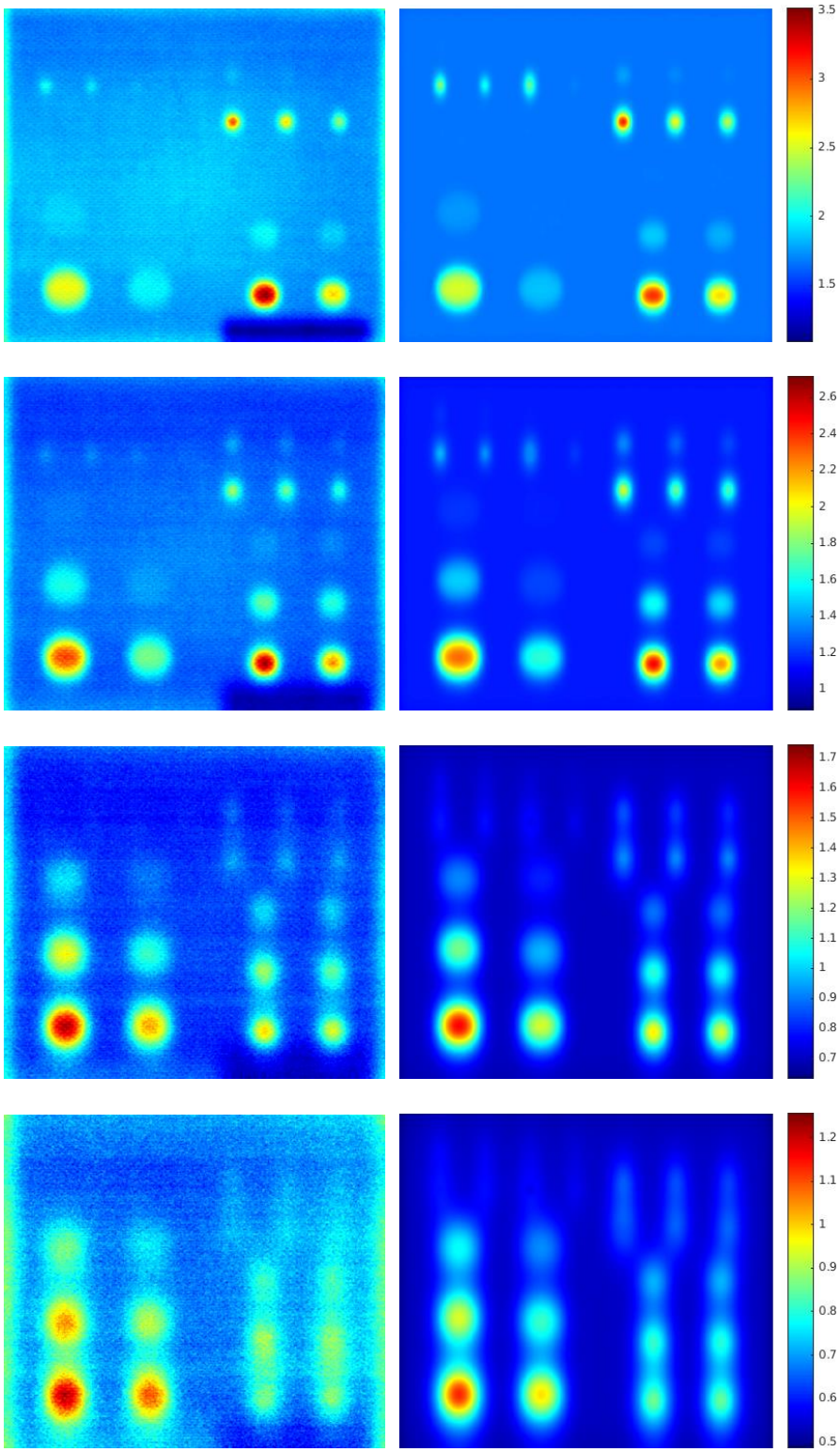

Fig. 2. Comparison of measurements (left column) and simulation (right) of CFRP UD. The pictures show the temperature increase 5 s, 10 s, 25 s and 40 s after the flash from top to bottom. Note that the temperature ranges change over time, such that the color coding changes. For measurements and simulations, the temperature axes are scaled same without any correction factor.

3. Reconstruction

3.1 PDE-based Identification of Material Parameters

To obtain a good match between simulation and measurements, accurate knowledge of material parameters is important. We use a Gauss-Newton method [9] to compute estimates of unknown or only approximately known parameters p. More precisely, we aim at minimizing the Tikhonov-regularized least-squares functional

$$\min \|F(p)\|_2^2 + 10^{-4}\|p - \bar{p}\|_2^2$$

where $F(p)$ denotes the difference in the surface temperature evolution between measurement and simulation. For simplicity, the required derivative of F is computed by finite differences. Nominal values $\bar{p}$ are either coming from measurements, as is the case for thermal diffusivity $\alpha = \lambda/(\rho c)$, or are taken from literature. The source of the values is attributed in Table 1 and 2. Note that the simulation does not use the thermal diffusivity, but heat conductivity λ, density ρ and heat capacity c as individual parameters.

Parameter identification for Epoxy-resin was conducted for specific heat capacity c and power density Q, using measurements of thermal diffusivity α to compute the specific heat conductivity from the initial heat capacity, see Table 1 for the results. Measurements of the temperature on the whole surface over a time interval of 5s after heating were used in the objective function.

Table 1. Material parameters for Epoxy-resin

	Epoxy	
Parameter	nominal	identified
Q [W/m²]	1,040,000±40,000[1]	1,007,945
α [m²/s]	along z: $(1.3 \pm 0.2) \cdot 10^{-7}$ used for all directions	not identified; $\lambda = 0.25$ used for all directions
c [J/(kg K)]	1700	1674.9

[1] Calculated from the measured energy density of 0.27 J/cm² and the flash duration of 2.0 ms (half time)

For CFRP UD, not the whole surface temperature could be used in the objective function, due to unmodeled external influences in the measurements (label, boundary influences, see Figure 2). Instead we aimed to minimize the temperature deviation during the first 50 s of cooling in a rectangular region bounded by the center points of the six largest flat bottom holes. Identified parameters were heating power, heat capacity and heat conductivity, the latter individually in x-, y-, and z-direction. Only the product of density and heat capacity enters the heat equation, such that density was not identified. As nominal values for the heat conductivity, values derived from measured diffusivity as well as values computed due to [8] were used (marked a) and b) in Table 2). Figure 3 shows a comparison of measurement and simulation results for 10 s and 25 s after flash heating for example a). While the temperature using identified parameters is closer to the measurement in the beginning than the one using the nominal values, the temperature is too low in the later frames. Figure 3 shows that for the nominal parameters, the simulated temperature is too high compared to the measurements. As only part of the surface is considered in computing the fit, and the coefficient of convective heat transfer is not adapted, lateral heat flow might be overestimated to compensate for too little cooling due to convection.

Table 2. Material parameters for CFRP UD

	CFRP UD		
Parameter	nominal	identified a)	identified b)
Q [W/m²]	1,040,000±40,000[1]	995,180	995,060
α [m²/s]	along x: $(7 \pm 2) \cdot 10^{-7}$ along y: $(1.0 \pm 0.3) \cdot 10^{-6}$ along z: $(3.5 \pm 2.0) \cdot 10^{-7}$		
ρc [J/(m³K)][2]	1 625 128.5	1 581 790.5	1 608 528.5
λ [W/(m K)] a)[3]	(1.087, 1.6284, 0.5454)	(5.282, 6.249, 0.527)	
λ [W/(m K)] b)[3]	(0.7645, 4.7991, 0.5123)		(5.177, 6.536, 0.536)

[1] Calculated from the measured energy density of 0.27 J/cm² and the flash duration of 2.0 ms half time.
[2] Note that the initial guess for the heat capacity is computed by averaging the heat capacities from matrix and fiber materials according to their volume fraction.
[3] See text for an explanation of the identified parameters a) and b).

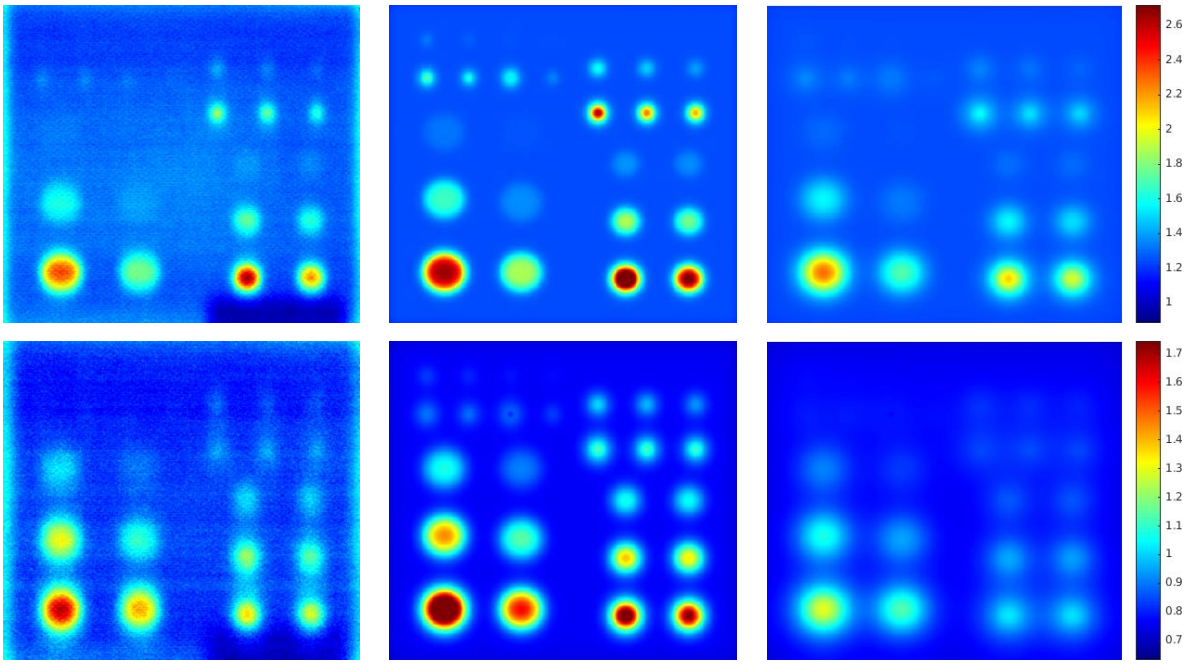

Fig. 3. Measurement (left) and simulation results with nominal (middle) and identified diffusivity (right) for example a).Top row: 10s past heating, bottom row: 25s past heating. The temperature is depicted color-coded, it is scaled to the same range for each row.

At the solution, the eigenvalues and eigenvectors of $F'(p)^T F'(p)$ give some information about the reliability with which the parameters can be identified. In the example considered here it turns out that the heating power density Q can be identified quite well, and the heat capacity with sufficient confidence. Lateral heat conductivity is somewhat less reliably identified, and the value for the heat conductivity in z direction is rather not to be trusted.

One important parameter in the model, which was not included in the parameter estimation, is the coefficient of heat transfer in the boundary condition. This parameter can be expected to correlate with the heat conductivity, and might therefore affect the expected reliability of estimating λ. Together with the identification of the spatial distribution of heating power this will be addressed in future work.

3.2 Geometry Identification

Besides identification of material parameters, the reconstruction of the geometry of the test specimen, especially the often inaccessible rear surface, is of interest. Mathematically, this can be seen as a shape optimization problem. For practical applicability, the treatment as such a PDE-constrained optimization problem is not possible, as this would require several computationally expensive PDE solutions. Alternatively, several heuristics are available for homogeneous isotropic objects.

The envelope method [10] is based on 1D analytical solutions for the heat equation, with an extension to take lateral heat flow into account. It assumes isotropic heat conductivity. Then, points on the rear surface or defects contributing to a temperature increase at the front surface compared to the solution of the heat equation for a 1D semi-infinite body lie on parabolas. As expected, for Epoxy-resin the reconstruction of flat bottom holes works quite well, see Figure 4. In CFRP, lateral heat flow is governed by the anisotropy of diffusivities, depending on the direction of the thermal wave propagation with respect to the fiber direction, such that direct application of the envelope algorithm is not possible.

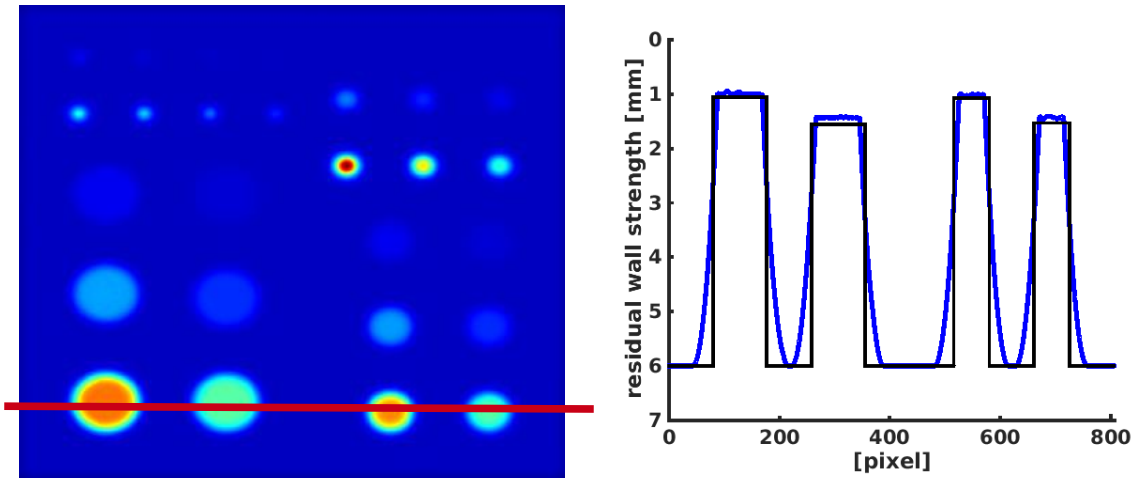

Fig. 4. Reconstruction of flat bottom holes from Epoxy-resin simulation using the envelope algorithm. The line in the left picture indicates the cross section for which the reconstruction is shown on the right. The reconstructed residual wall strength of the holes is within 0.1 mm of the true value.

A second approach, developed in [11] to reduce noise in measurement data, is based on the decomposition of the surface temperature into Greens function solutions, modeling contributions of heating, surrounding temperature and heat wave reflections from defects in different depths as an additive superposition. A least squares fit is computed to find the nonnegative coefficients of the Greens functions, see Figure 5. As before, this is based on 1D solutions of the heat equation, and has to be adapted to the anisotropic case. Nevertheless, a direct application to the CFRP temperature measurements gives reasonable results, at least for the larger flat bottom holes close to the surface.

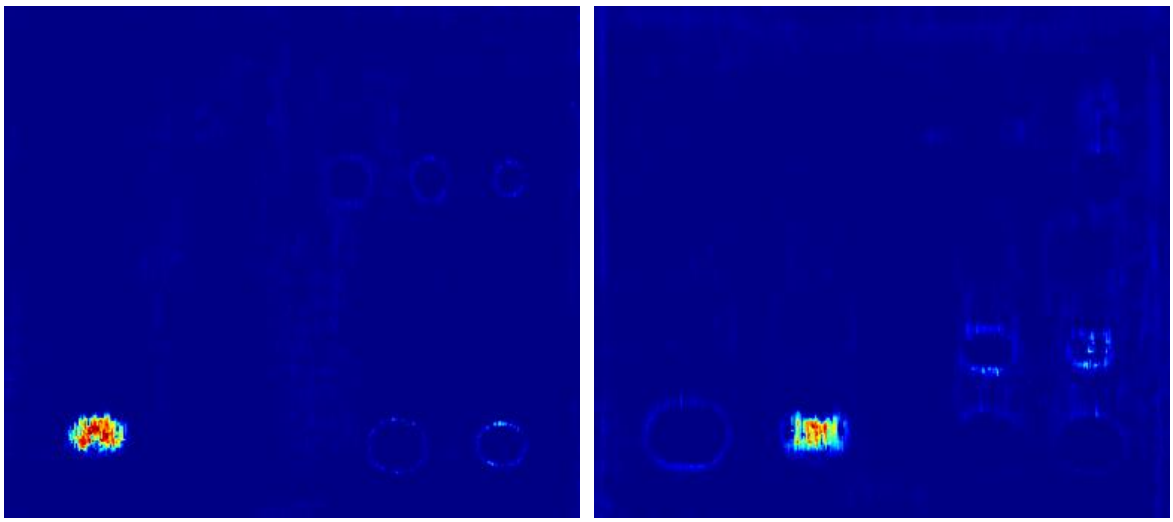

Fig. 5. Coefficients for the Greens function modeling contribution from a rear in depth 1.2 mm (left) and 1.7mm (right). The locations correspond to the centers of the largest defects (top left and second from left in first row in Fig.1), which have a true residual wall strength of 1.5 mm and 2.1 mm. Note that the anisotropic heat conductivity is not taken into account here, yet.

Starting from these preliminary results, future work will deal with the extension of such methods to deal with anisotropic heat flow in fiber reinforced composites.

4. Conclusion

The simulation results indicate that also for anisotropic composite materials, a careful finite element simulation of the heat transfer can reproduce the camera measurements rather well. Identifying material parameters, on the other hand, is much harder. While some parameters or parameter combinations can be identified quite reliability, others cannot be determined from the measurement. The latter effect may, however, not be an inherent property of the inverse thermography problem, but may reflect quantitative errors in the model, e.g., in the boundary conditions.

As a simulation with sufficient accuracy is computationally expensive, fast heuristics are needed for practical purposes. In particular, the envelope algorithm appears to be promising for detecting back surface defects and strong delaminations, but needs to be adapted to anisotropic heat conductivity. The Greens functions approach, on the other hand, gives quantitative less reliable results, but is attractive as it, in principle, should be able to detect layered delaminations, e.g., impact damages.

References

[1] X. Maldague and S. Marinetti, Journal of Applied Physics 79, 2694 (1996)
[2] S. M. Shepard, Proceedings of SPIE 4360, 511 (2001)
[3] W. J. Parker, R. J. Jenkins, C. P. Butler, and G. L. Abbott, Journal of Applied Physics 32, 1679 (1961), doi: 10.1063/1.1728417
[4] R. Krankenhagen and C. Maierhofer, Infrared Physics & Technology 67, 363 (2014), doi: 10.1016/j.infrared.2014.07.012
[5] P. Bison, F. Cernuschi, and S. Capelli, Surface and Coatings Technology 205, 3128 (2011), doi: 10.1016/j.surfcoat.2010.11.013
[6] M. Weiser, M. Röllig, R. Arndt, and B. Erdmann, Heat Mass Transfer 47, 1419-1428 (2010)
[7] S. Götschel, M. Weiser, and A. Schiela, Advances in DUNE, 101-112 (2012)

[8] F. Lopez, V. de Paulo Nicolau, C. Ibarra-Castanedo, and X. Maldague, International Journal of Thermal Sciences 86, 325-340 (2014)
[9] P. Deuflhard. Newton Methods for Nonlinear Problems. Affine Invariance and Adaptive Algorithms. Springer (2006)
[10] S. Götschel, M. Weiser, C. Maierhofer, R. Richter, and M. Röllig.
in: O. Büyüköztürk et al. (Eds.) Nondestructive Testing of Materials and Structures, RILEM Bookseries, Vol. 6, 83-89 (2013)
[11] S. Götschel, M. Weiser, C. Maierhofer, R. Richter. Proceedings of the 11th QIRT Conference (2012)